Contents lists available at ScienceDirect

Chemical Engineering Research and Design

journal homepage: www.elsevier.com/locate/cherd

Techno-economic assessment of the production of phthalic anhydride from corn stover

Sara Giarola[a], *Charles Romain*[b], *Charlotte K. Williams*[b], *Jason P. Hallett*[c], *Nilay Shah*[c,*]

[a] *Earth Science & Engineering, Imperial College London, SW7 2AZ, UK*
[b] *Chemistry Department, Imperial College London, London SW7 2AZ, UK*
[c] *Chemical Engineering Department, Imperial College London, London SW7 2AZ, UK*

ARTICLE INFO

Article history:
Received 15 July 2015
Received in revised form 15 October 2015
Accepted 20 October 2015
Available online 31 October 2015

Keywords:
Biorefinery
Corn stover
Phthalic anhydride
Simulation

ABSTRACT

Phthalic anhydride is used worldwide for an extremely broad range of applications spanning from the plastics industry to the synthesis of resins, agricultural fungicides and amines. This work proposes a conceptual design of a process for the production of phthalic anhydride from an agricultural residue (i.e. corn stover), energy integration alternatives as well as water consumption and life cycle greenhouse emissions assessment. The techno-economic and financial appraisal of the flowsheet proposed is performed. Results show how the valorization of all the carbohydrate-rich fractions present in the biomass as well as energy savings and integration is crucial to obtain an economically viable process and that it is in principle possible to produce renewable phthalic anhydride in a cost-competitive fashion with a lower impact on climate change compared to the traditional synthetic route.

1. Introduction

World phthalic anhydride (PA) demand is mainly driven by end-use applications such as phthalates-based plasticizers (62%), resins (38%, e.g. alkyd and UPE resins) and, to a lesser extent, dyes (mcgroup, 2015). Despite emerging trends of plasticizers manufacturing to become increasingly phthalate-free, the PA market currently accounts for more than 3 million tonnes per year and is expected to grow at about 2.4% per year in the near term (IHS, 2015).

Until the 1960s PA was based on coal-tar naphthalene oxidation processes. In the 90s, most of the PA was obtained from o-xylene, which can be separated from mixtures of xylenes containing roughly one third o-xylene and two thirds p-xylene. Although most of the PA production plants typically envisage possibilities of switching between the two feedstocks, the manufacturing costs are necessarily linked to fossil (mostly oil) price fluctuations. As such, a renewable route to PA would be highly encouraged as a first step towards a completely bio-based production of polyesters or polycarbonates (Winkler et al., 2015).

The development of chemicals manufactured from renewables (i.e. bio-based chemicals) has been receiving an increasing interest not only due to environmental policies (at both national and international levels) but also due to initiatives of private companies (like Cargill and BASF) (Golden and Handfield, 2014). The emerging bioeconomy growth is currently led by the bio-plastics sector but is expected to soon include specialty chemicals up to a significant extent (Arundel and Sawaya, 2009). The replacement of petroleum-derived products with bio-based ones is a promising answer to energy security and climate change issues. As a matter of fact, a large number of potential applications of biomass to produce bulk and niche chemicals have already been disclosed by chemistry and biotechnology researchers (EC, 2006) but concerns regarding the technical and practical feasibility of large-scale biorefining infrastructures still hinder the expansion of these systems.

Bio-ethanol has received considerable attention as a basic chemical and fuel additive. The extensive research on bioethanol has revealed that process intensification is essential to cut the production costs and ensure process viability. He and Zhang (2011) designed and optimised a thermo-chemical process for ethanol production where biomass wood chips were dried and gasified. The syngas produced was then cleaned and converted into alcohols. Ethanol and a mixture of higher alcohols were purified and sold. He and Zhang (2011) assessed the process in

* *Corresponding author*. Tel.: +44 020 7594 6621; fax: +44 020 7594 6606.
E-mail address: n.shah@imperial.ac.uk (N. Shah).
http://dx.doi.org/10.1016/j.cherd.2015.10.034

terms of carbon and CO conversion, ethanol yield, synthesis selectivity and ethanol production cost. The results showed that major contributions to the production cost are from biomass feedstock and syngas cleaning. Cost-competitive ethanol production can be realized with optimal systematic conguration and heat integration as well as high value by-products.

In the biorefining context, though, only a limited number of studies have proposed rigorous techno-economic assessments of selected bio-based chemicals. Trippe et al. (2011) proposed a techno-economic assessment of biomass-derived slurry (bioliq) in a potential industrial scale entrained flow gasifier. They emphasised that the role of syngas in future bioeconomy allowed a wide variety of fuels and chemicals using specific catalysts, and that feedstock cost mainly affected production costs.

The integration of lactic acid production in the sugarcane-based biorefinery was targeted by Sikder et al. (2012). Lammens et al. (2012) have developed a techno-economic feasibility analysis of bio-based products derived from glutamic acid.

Haro et al. (2013) proposed the conceptual design of 12 alternatives developed around the concept of an indirect ethanol production biorefinery using dimethyl ether (DME) as an intermediate. They studied the polygeneration of high-value chemical products (methyl acetate and H_2), liquid transportation fuels (ethanol and DME) and electricity. For the market price of products the internal rate of return was always above 20% for process concepts based on DME carbonylation. In the most profitable scenario, a rate of return of 28.74%, was obtain where methyl acetate, DME and power were produced.

Cok et al. (2014) proposed an energy and greenhouse gas emissions assessment of bio-based succinic acid obtained from carbohydrates. Kim et al. (2014) performed a conceptual design and studied the economics of ethanol production using starch and lignocellulosic biomass as starting feedstocks. They showed that the economics of the system were significantly improved when the efficiency in the use of biomass was augmented. They combined several pretreatment processes (i.e. the dilute acid and aqueous ammonia pretreatments), and proposed a process of waste media containing xylose for the production of 7-aminocepha-losporanic acid. Tang et al. (2014), finally, explored in their review the role of GVL (γ-valerolactone), obtainable by selective hydrogenation of lactic acid and its esters, as a solvent for producing chemicals and building-block for generation biofuels. A cost-effective process for producing lactic acid from lignocellulosic biomass was shown as the real bottleneck for the GVL production in a large scale, because of its strong acidity and low volatility.

A renewable route to PA was investigated at a lab scale by Mahmoud et al. (2014) using biomass-derived furan (F) and maleic anhydride (MA). This represented a promising avenue for the production of PA from diverse routes compared to the traditional fossil-based one at the same time using residual feedstock (the so-called second generation biomass) whose exploitation would not interfere with the food supply chain. In this work, the originally developed conceptual design proposed by Giarola et al. (2015) for the production process of PA from corn stover, is extended proposing pinch analysis and energy integration solutions. Additional product sales are also modelled as a means to improve the profitability of the system (levulinic, maleic anhydride and formic acid, i.e. LA, MA, FA). The full techno-economic assessment, including economic and cash flow analyses as well as the water consumption and greenhouse gas (GHG) emissions appraisal of the process are presented.

2. Materials and methods

2.1. Gas-phase oxidation

PA is produced via the oxidation reaction occurring at about 360–390 °C (Lorz et al., 2012) of:

- o-xylene, with a heat of reaction between 1300 and 1800 kJ/mol of o-xylene and expected yields of 110–112 kg PA/100 kg o-xylene
- naphthalene, with a heat of reaction of 2100–2500 kJ/mol and yields usually not exceeding 98 kg PA/100 kg naphthalene; carbon dioxide is a co-product.

The traditional source for PA production was coal-tar naphthalene, which could be available at adequate purity only at high costs. Recently, the PA manufacturing has shown a shift towards o-xylene use, for the more attractive yields, availability and cost. As a major drawback, the process economics became more exposed to the main feedstock price variations as well as the high volatility of mixed xylenes in the international market (ICIS, 2015). In order to hedge this risk, some plants allow o-xylene-naphthalene switching or include a xylene separation plant.

The first patent (BASF in 1896) used concentrated sulphuric acid in the presence of mercury salts to perform the oxidation, but the major advancement in PA manufacturing occurred when the first vapour-phase process spread across the world with the development of highly selective catalysts based on vanadium pentoxides.

When o-xylene is the feedstock, it is first vaporized, mixed with hot air and passed through a fixed-bed tubular reactor where the oxidation takes place. The exothermic heat is removed by a molten salt bath circulated around the reactor tubes and transferred to a steam generation system.

When a naphthalene-based feedstock is used, vaporized naphthalene and compressed air are transferred to a fluidized bed reactor and oxidized in the presence of a catalyst. The cooling tubes transfer the exothermic heat from the catalyst bed to produce high-pressure steam.

The reactor effluent gases are filtered to recover the catalyst, precooled and passed through a liquid condenser, first, and to a switch condenser system, then, where the PA is condensed on the finned tubes as a solid. The switch condensers are cooled by a heat-transfer oil in an automated switching cycle: during the cooling cycles, PA crystals form while, during the heating cycle, the deposited PA is melted and collected from the condenser tubes in a storage tank. The exhaust gases still contain byproducts and small quantities of PA and must be cleaned by scrubbing with water, or catalytically or thermally incinerated. If scrubbing with water is employed, it is possible to concentrate the maleic acid, and, from the scrubbing solution maleic anhydride. The crude liquid is transferred to a continuous thermal/chemical treatment system, which converts the phthalic acid formed into the anhydride, then purified (99.8% wt.) in a continuous two-stage vacuum distillation system.

Current industrial plants exhibit a good variety of technological solutions operating at different ranges of o-xylene loadings (from 80 g/m^3 (STP) in the Alusuisse - Ftalital LAR (low air ratio) process, up to 105 g/m^3 (STP) in the BASF process).

2.2. A novel synthesis to PA based on biorenewables: input assumptions

In this work, a generic, simplified PA production process (displayed in Fig. 1) using corn stover as raw material was developed and simulated by means of a process simulator (Aspen Plus^{TM}). An energy optimisation was then performed according to the principles of the pinch analysis. An environmental appraisal of the GHG emissions of the process using a life cycle approach was also conducted. The water consumption of the system was also estimated. Table 1 reports

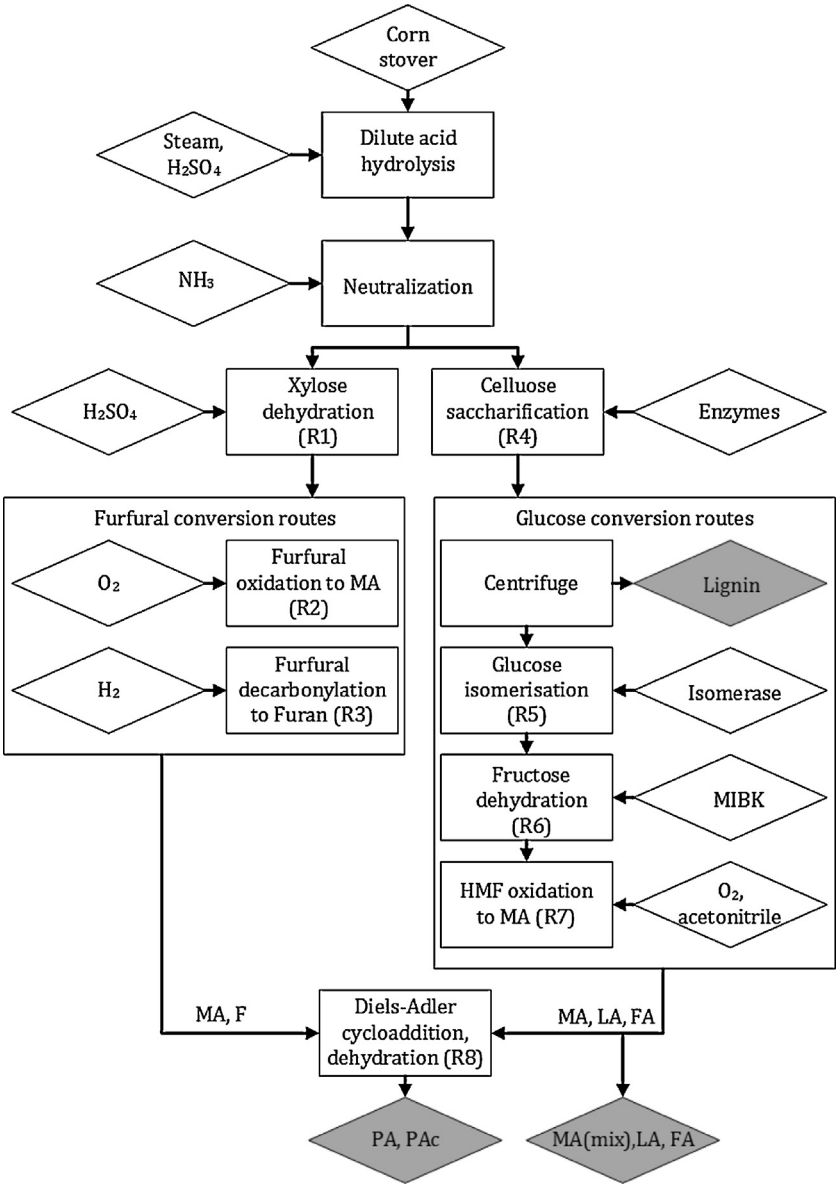

Fig. 1 – PA process overview.

the composition of the feedstock used in this study (Humbird et al., 2011).

The process conceptual design was developed aiming at the full exploitation of the biomass macro-components (i.e. cellulose, hemicellulose and lignin). It was based on an extensive survey of technical chemistry solutions (i.e. experimental and industrial) and sensitivity analysis to screen promising process configuration alternatives. The simulation mainly uses component physical properties internal to the software as well as property data developed at NREL (Humbird et al., 2011).

Vapour–liquid equilibria were described using the NRTL model, considering O_2, N_2, CO_2, CH_4 and H_2 as components following Henry's Law.

Liquid–liquid extraction systems were modelled using the UNIFAC-Dortmund property model according to Román-Leshkov (2014).

Reactors have been modelled using fixed conversion units. A rigorous modelling of kinetics was outside the scope of the work.

Table 1 – Feedstock composition.

Component	Mass fraction (dry basis)
Cellulose	0.3895
Galactan	0.0159
Mannan	0.0069
Xylan	0.2831
Arabinan	0.0476
Lignin	0.1346
Acetate	0.0635
Protein	0.01
Ash	0.0489

2.3. *Process overview*

The plant was designed to treat a nominal capacity of 104,167 kg/h of milled corn stover at 20% wt. of bulk moisture content for the production of PA. This plant size would be compatible with a 50-mile biomass collection radius, which is considered suitable for a lignocellulosic biorefinery (Humbird et al., 2011). The process was divided into six key areas:

- Feed Handling. The feedstock (i.e. milled corn stover) is delivered to the feed handling area from which it is

conveyed to the pretreatment reactor. This section was not simulated in Aspen Plus™.

- Pretreatment and conditioning. The biomass is treated with a co-current dilute-acid pretreatment to make the hemicellulose sugars and the cellulose available for subsequent reactions. Ammonia-based conditioning is used for the hydrolyzate pH neutralisation.
- Reaction. This section is segmented into parts specifically designed to treat each biomass fraction, after the lignin is separated from the hydrolyzate. The cellulose is first saccharified and isomerised. It is converted into 5-Hydroxymethylfurfural (HMF) and, finally, maleic anhydride (MA). Hemicellulose sugars are reduced to furfural by adding sulphuric acid. Furfural is converted into a parallel scheme of reactions: it partly goes into either furan (F) production or MA. MA and furan (F) react for the production of PA on an equimolar basis.
- Furfural purification. The neutralised hydrolyzate obtained is treated with sulphuric acid for being converted into furfural, which is then distilled off and concentrated.
- HMF purification. HMF is separated and extracted from the aqueous mixture by adding MIBK and creating a biphasic system.
- Product purification. This section includes all the major reactants (i.e. MA, F) and products purification (i.e. PA, formic acid FA).

2.4. *Selected reactions*

This section is devoted to the description of the reaction paths modelled. Reactors tags and streams refer to the representation of the process as reported in Fig. 2. The flowsheet of the recovery sections is reported in Figs. A.1–A.3.

A summary of reactors operating conditions, reactions and main reactant conversions is reported in Table A.1.

In order to make the hemicelluloses available, the biomass must undergo pretreatment, which was modelled according to Humbird et al. (2011). As such, in the presteamer M1 milled corn stover is mixed with steam (at 7 atm and 100 °C). It is then treated in the pretreatment reactor M2 (operating at 5.7 atm 158 °C) with dilute sulphuric acid (2.21% of inlet solids by weight). Under these conditions, 90% of the xylan is assumed to convert into xylose; also side reactions are occurring as listed below (r1)–(r7).

At this stage, the hydrolyzate is treated in a neutralisation (M3, operating at 77.1 °C and 5.7 atm) and a reacidification section (M4, operating at 77.4 °C and 3.4 atm). Ammonia is first added to convert acids into ammonium sulphate and acetates; then the amount in excess is neutralised with sulphuric acid into ammonium sulphate (r8)–(r11).

Solids (i.e. unreacted hemicellulose, cellulose and lignin) are filtered in the pressure filter FP1 and separated from the liquid hydrolyzate, assuming a unitary separation efficiency.

$$\text{cellulose} + H_2O \xrightarrow{H_2SO_4} \text{glucose} \quad (1)$$

$$\text{cellulose} \xrightarrow{H_2SO_4} \text{HMF} + 2H_2O \quad (2)$$

$$\text{xylan} + H_2O \xrightarrow{H_2SO_4} \text{xylose} \quad (3)$$

$$\text{xylan} \xrightarrow{H_2SO_4} \text{furfural} + 2H_2O \quad (4)$$

$$\text{acetate} \xrightarrow{H_2SO_4} C_2H_4O_2 \quad (5)$$

$$\text{HMF} + 3H_2O \xrightarrow{H_2SO_4} \text{TAR} \quad (6)$$

$$\text{furfural} + 3H_2O \xrightarrow{H_2SO_4} \text{TAR} \quad (7)$$

$$C_2H_4O_2 + NH_3 \rightarrow NH_4^+C_2H_3OO^{2-} \quad (8)$$

$$H_2SO_4 + 2NH_3 \rightarrow (NH_4^+)_2SO_4^{2-} \quad (9)$$

$$\text{xylose} \rightarrow \text{TAR} \quad (10)$$

$$H_2SO_4 + 2NH_3 \rightarrow (NH_4^+)_2SO_4^{2-} \quad (11)$$

The C5-sugars in the hydrolyzate (mainly xylose) are dehydrated to furfural in R1 (r12)–(r13). The reaction system was

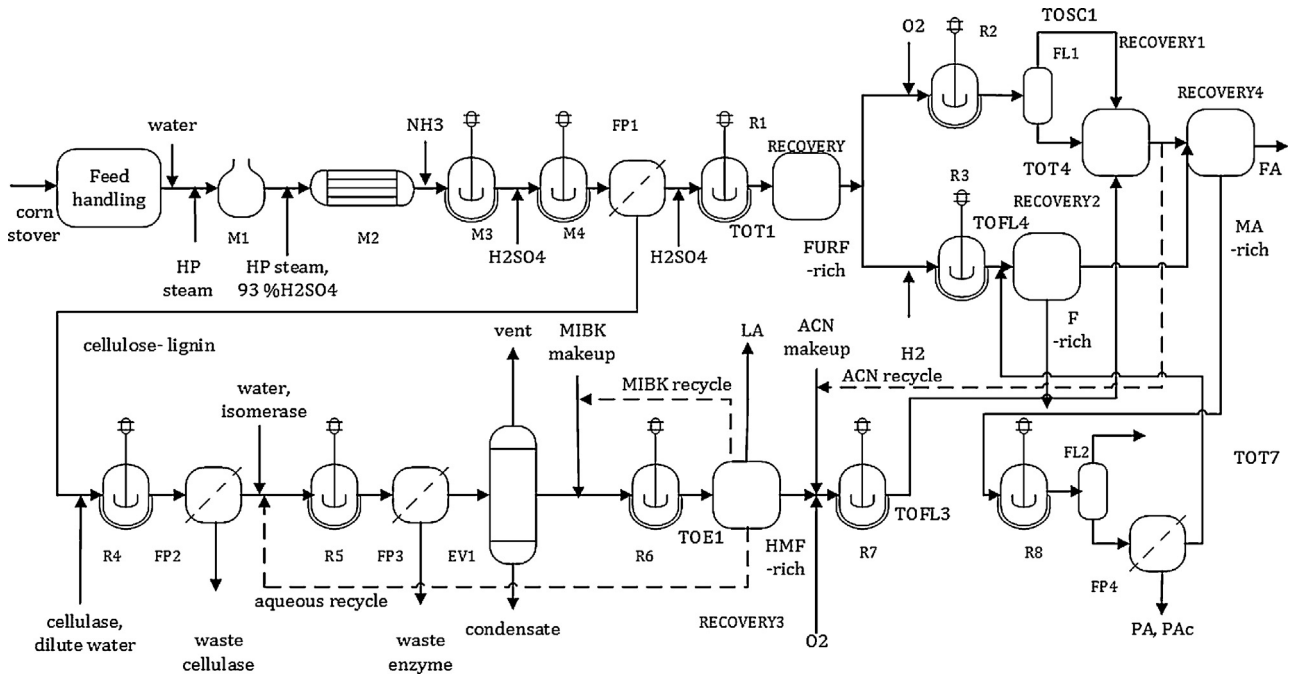

Fig. 2 – PA process: detail on reactor scheme.

modelled according to the setup reported by Mandalika and Runge (2012) who achieved high product yields and low degradation by performing a batch reactive distillation, sulphuric acid-catalyzed, of several pentosan-rich biomass, such as miscantus or corn stover. In the experimental procedure, furfural was immediately distilled off avoiding condensation reactions with sugars into humins. The selection of this reaction path allowed a homogeneous reaction medium and the continuity with the one used in the pretreatment. The reaction system was modelled in Aspen Plus™ using two separate units: a fixed conversion reactor (operating at 168.5 °C and 7.6 atm) followed by a distillation tower.

Two alternative conversion routes for furfural have been considered:

- in R2, furfural is oxidized in presence of oxygen (nearly atmospheric pressure and 319.85 °C) over VO_x/Al_2O_3 catalysts with 73% selectivity to MA (Alonso-Fagúndez et al., 2012), while side-reactions would mainly yield to 2-furanone. A simplified reaction path was modelled (r14)–(r16);
- in R3, furfural is converted into F (at 90.9% yield) via vapour-phase decarbonylation (atmospheric pressure and 310 °C) over Pd-Li-alumina catalyst promoted with cesium carbonate. The reaction path (r17)–(r19) was modelled considering experimental yields as reported by Ozer (2014). The main by-products were furfuryl alcohol and tetrahydrofuran (THF).

A sensitivity analysis was carried out at a preliminary stage of the simulation to determine the relative merit (using the undiscounted profit as performance metric) of alternative product portfolios as achieved from varying the split between the two furfural-related avenues. The best split ratio between the two conversion paths for furfural was found to privilege F production (60% of the overall furfural rate).

$$\text{xylose} \xrightarrow{H_2SO_4} \text{furfural} + 3H_2O \quad (12)$$

$$\text{furfural} + 3H_2O \xrightarrow{H_2SO_4} \text{TAR} \quad (13)$$

$$\text{furfural} + 0.5O_2 \rightarrow \textit{furan} + CO_2 \quad (14)$$

$$\text{furan} + 0.5O_2 \rightarrow \text{furanone} \quad (15)$$

$$\text{furanone} + O_2 \rightarrow \text{MA} + H_2O \quad (16)$$

$$\text{furfural} \rightarrow \text{furan} + \text{CO} \quad (17)$$

$$\text{furfural} + H_2 \rightarrow \text{furfuryl alcohol} \quad (18)$$

$$\text{furan} + 2H_2 \rightarrow \text{THF} \quad (19)$$

The neutralised hydrolyzate (stream *cellulose-lignin*) is diluted with water to a 20% solid loading before entering the saccharification (R4) which takes place at 48 °C. The main reaction (r20) modelled according to Humbird et al. (2011) allows 90% conversion of cellulose into glucose, adding 2% of cellulase per unit of inlet cellulose by weight.

The C6 sugars (i.e. glucose) produced from the saccharification are separated from the residual solids through the pressure filter FP2. These sugars are involved in the reaction branch leading to MA via HMF. Since the glucose can be dehydrated into HMF only at low yields when the reaction is carried out in an aqueous medium, preliminary glucose isomerisation to fructose is recommended. In this process design, the isomerisation (the rate-limiting step) occurring in R5, was modelled involving the reaction (r21) (Gaily et al., 2010), operating the system at 10% glucose solution and 60 °C using isomerase enzyme (15% by weight of the treated glucose). The spent enzyme is separated in the pressure filter FP2. The unreacted glucose was recycled to the isomerisation reactor. A triple effect evaporator system was employed (EV1 in Fig. 2) which operates at 0.35, 0.2 and 0.09 atm to concentrate the feed to reactor R5 from 10 to 30% wt. of sugars.

$$\text{cellulose} + H_2O \rightarrow \text{glucose} \quad (20)$$

$$\text{glucose} \rightarrow \text{fructose} \quad (21)$$

The obtained fructose is then dehydrated in R6 to HMF as proposed by Román-Leshkov (2014), who used a biphasic system where the HMF produced in the aqueous medium (using hydrochloric acid as a catalyst) was extracted into an organic phase. Among the alternatives proposed by the authors, a good balance of fructose conversion (91%) and HMF selectivity (60%) was achieved using MIBK as the extractive agent with a volumetric ratio against the liquid phase equal to 1.51. The reaction path of the unit R6 was modelled as shown in (r22) and (r23), with LA and FA as major by-products. MIBK was modelled as an extractive agent, thus neglecting hydrochloric acid in the process. Alternative extractive agents proposed by Román-Leshkov (2014) (i.e. mixtures of MIBK and 2-buthanol) did not prove to be more efficient from the process system modelling perspective as they would introduce an additional azeotrope with water (i.e. 2-buthanol-water).

$$\text{fructose} \rightarrow \text{HMF} + 3H_2O \quad (22)$$

$$\text{HMF} + 2H_2O \rightarrow CH_2O_2 + C_5H_8O_3 \quad (23)$$

The HMF is then oxidized yielding MA at 52% over $VO(acac)_2$ catalysts according to the scheme proposed by Du et al. (2011). The reaction occurs in the unit R7 and involves the oxidation of HMF to MA as main reaction (r23) and MA hydration to its corresponding acid (r25). The additional by-products into which HMF is reported to degrade (2,5-dyformylfuran, esters, humins) have been modelled as side streams leaving the reactor. The reaction medium has been simulated considering just acetonitrile as a solvent, as it accounts for the largest share in the solution medium (82% wt.).

$$\text{HMF} + 2O_2 \rightarrow \text{MA} + 2CH_2O_2 \quad (24)$$

$$\text{HMF} + 3O_2 \rightarrow \text{MAc} + 2CO_2 + H_2O \quad (25)$$

PA was produced at lab scale in a two reaction steps (Mahmoud et al., 2014): a Diels-Adler cycloaddition between F and MA at room temperature and solvent free conditions (yielding 96% of oxabornene dicarboxylic anhydride) was followed by the dehydration of the intermediate at 79.85 °C in a mixture of sulfonic carboxylic anhydrides in methanesulfonic acid. The experimental procedure has been modelled (R8) in a simplified manner involving two main reactions at room temperature: one between F and MA into PA and the formation of the corresponding acid (PAc) (r26) and (r27). The presence of the anhydrides mix was not modelled in the vapour–liquid equilibrium due to the lack of property characterisation. The reactor effluent is first flashed (in FL2, operating at 60 °C and

1.5 atm) then PA and PAc are separated in a pressure filter (FP4). The final PA crystallization step was not modelled in Aspen Plus™.

$$\text{furan} + \text{MA} \rightarrow \text{PA} + \text{H}_2\text{O} \quad (26)$$

$$\text{PA} + \text{H}_2\text{O} \rightarrow \text{PAc} \quad (27)$$

2.5. *Separation system*

The separation system was intended to recover the final products for sale and the chemical intermediates before being sent to the corresponding reactors where they are transformed, as described in Section 2.3.

The binary interactions parameters have been regressed from experimental data for the major azeotropic systems (*water-ACN*, (Maslan and Stoddard, 1956), *water-FA*, (Ito and Yoshida, 1963), *water-THF* (Pick, 1972)).

The UNIFAC-Dortmund property model was implemented assuming the functional groups for the compounds involved in the extraction units. In particular:

- *fructose* was modelled with 1 4-bonded C group, 4 OH-groups, 2 CH_2 groups, 2 CH groups, 1 aldehydic group
- *glucose* was modelled with 4 OH-groups, 1 CH_2 group, 4 CH groups, 1 aldehydic group
- *HMF* was modelled using 1 CH_3OH and 1 furfural group (Román-Leshkov, 2014)
- *LA* was modelled with 2 CH_2 groups, 1 COOH group, 1 CH_3CO (ketone) group

The recovery system hereby shows two major changes compared to the original design proposed in Giarola et al. (2015):

- the stabilizer which originally followed reactor R8 was replaced by a simple flash (FL2);
- the MIBK recovery was redesigned with the addition of series of extractors and the removal of a distillation column which preceded, in the previous design, the pressure swing distillation (PSD) for the FA purification.

The detailed description of the separation system is organized per recovery section:

- Recovery: In the outlet stream from reactor R1, furfural is available at about 7.7% wt. and needs purification before being sent to the F and MA synthesis branches. This separation is challenged by the presence of an azeotrope in the system *water-furfural*. Fig. A.1 gives an explanatory representation of the separation system modelled, which was developed after (Arnold and Gross, 1964) and enabled a high purity furfural stream. It is composed of a first tower (T1) which separates a bottom waste stream rich in water and salts. The distillate is then purified to extract pure furfural (T2 bottoms) via a PSD sequence (T2, T3), with an intermediate decanter at 40 °C.
- Recovery 1: The outlet stream from reactor R2 is flashed first in FL1. FL1 and FL3 (receiving reactor R7 effluent, as shown in Fig. A.3) overhead vapours (35 °C, 1 atm) are mixed and treated in the scrubber SC1. SC1 overheads are vented, while bottoms are treated in a series of 3 distillation columns (T4, T5, T6) to break the *water-ACN* azeotrope. Adapting the scheme proposed by Presson et al. (1982), 97.1% of ACN at the purity of 95% wt. is recovered and recycled before the reactor R7. The separation scheme is reported in Fig. A.3.
- Recovery 2: As shown in Fig. A.3, the outlet stream obtained from furfural decarbonylation (R3) is cooled and flashed in FL4 (operating at 35 °C and 1 atm). FL4 vapours are sent to the water scrubber SC2. FL4, FL2 liquid effluent (TOT7) and SC2 bottoms are treated in the distillation tower T7, where F at 99.6% wt. is recovered and sent to the reactor R8.
- Recovery 3: This section concerns HMF purification and MIBK recovery following R6, as displayed in Fig. A.2. The outlet stream from R6 contains a biphasic system where MIBK is used to preserve HMF from mixing with water (Román-Leshkov, 2014). The extractor E1 only allows a coarse separation of HMF from MIBK (E1). Further treatment is required to recover the solvent and separate the HMF from byproducts:
  - the E1 organic phase is further concentrated with a series of evaporators (EV3) operating at 1.3, 0.4 and 0.013 atm. The condensates with a high fraction of HMF and LA are conveyed to the distillation column T8; the condensates at a higher concentration of MIBK undergo a further extraction (E2)
  - the E1 aqueous effluent stream is sent to a flash (FL5) operating at 70 °C, 0.17 atm, and to a subsequent extractor E3. An MIBK-rich stream is extracted and a second one rich in FA is obtained (TOT12);

  The MIBK-rich streams obtained from E3 as well as EV3 vapours, T8 distillate and E2, after being flashed in FL6 (17 °C, 0.013 atm), are recycled to reactor R6. The HMF-LA mixture contained in the T8 bottoms is separated in the distillation column T9: an LA-rich distillate is obtained, while the bottoms (rich in HMF) are sent to reactor R7.
- Recovery 4: As shown in Fig. A.3, MA is recovered from the columns T5 and T7 bottoms in the form of MAc and is treated into two series of evaporators (EV2):
  - the former sequence is composed of 4 evaporators operating at 1.18, 0.55, 0.13, 0.03 atm;
  - the second sequence is composed of 3 evaporators operating at 1.05, 0.34, 0.013 atm.

  The liquid effluent stream at 90% wt. of MAc dehydrates to MA. The MA-rich stream is further concentrated in a sequence of 2 evaporators (operating at 0.4, 0.1 atm) up to 84% wt. MA is further refined to a 95.2% wt. Purity in a first distillation column operating under vacuum (T10), where light compounds are removed overheads and sent to T12. Heavy compounds are separated in the bottom stream of column T11. An MA distillate at the purity of 99% wt. is recycled to reactor R8 where it reacts at equimolar basis to the F flows. The MA excess is sold at 97.7% wt. purity.
  The FA-rich streams (EV2 condensates and TOT12) are treated in a PSD module (T12, T13). T12 overheads are rich in FA at 90% wt. and are sold as process by-product. The separation scheme is reported in Fig. A.3.

The streams denoted *WWT* are generally water-rich streams obtained from columns and evaporator condensates as shown in Figs. A.1–A.3; they are processed in the waste water system. They contain 6% wt. of COD (Chemical Oxygen Demand), 86% of which (on a mass basis) is converted to biogas containing 51% mol. CH_4 and 49% mol. CO_2. All in all, the *WWT* streams would produce 228 g CH_4/kg COD removed (Humbird et al., 2011).

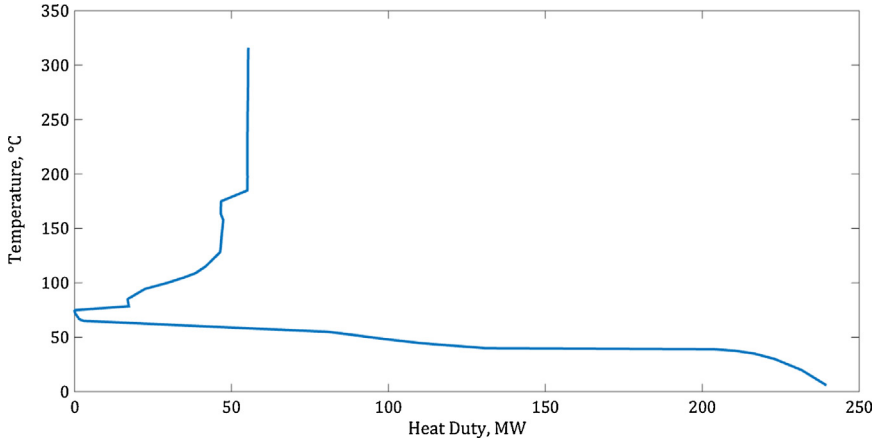

Fig. 3 – PA process: heat cascade.

2.6. *Heat cascade*

A pinch analysis was performed to improve the energy network of the system. The pinch technology approach (Linnhoff and Flower, 1978) offers a systematic methodology to obtain optimum energy integration of the process. First temperature and enthalpy data were gathered for the hot process streams (i.e. those that must be cooled), cold process streams (i.e. those that must be heated) from the process simulation. The minimum approach temperature was set to 10 °C.

The shifted temperature versus enthalpy graph (i.e. heat cascade) is shown in Fig. 3. The pinch point is at 74.85 °C. The minimum energy requirement was estimated as being equal to 55.4 MW of the hot utility and 239.1 MW of the cold utility.

To maximise the heat exchanged in the system, starting from the basic flowsheet a series of loops to tune the column pressure was performed in order to have all the towers operating either above or below the pinch. In doing so, one of the major constraints was connected to the product degradation at high temperatures. In particular, MAc would degrade to fumaric acid at a temperature of about 130 °C, which translates into irrecoverable loss of product. As such, T10 was constrained to operate at a very low pressure to balance both the needs (product integrity and energy savings). A compressor was used to increase the vapour distillate pressure of the tower T10 from 0.008 to 0.1 atm, thereby undergoing condensation mainly by compression with intermediate cooling down to 40 °C.

The detail of the operating conditions for towers and extractors is reported in Table A.2.

The amount of heat which needs to be externally provided to the plant (as shown in Fig. A.4 where temperatures of reboilers (as cold streams), condensers (as hot streams) as well as the heat of reactions were added to the heat cascade) was calculated as being equal to 311 MW. The left-over of solids/spent enzymes, biogas (obtained from the waste water treatment) and natural gas (NG) were fed to the combined cycle gas turbine and respectively contributed to 32%, 16% and 52% of the overall energy inlet. Steam and electrical efficiencies were assumed equal respectively to 55% and 30% calculated on the basis of inlet energy (IEA-ETSAP, 2005). This solution allowed a co-production of 170 MW of power alongside the raised steam (311 MW of high pressure steam and 85 MW of low pressure steam). As the plant power demand equals 18 MW, a net power surplus (152 MW) is generated and can be sold to the grid.

High and low pressure steam are produced with the combined-cycle gas turbine.

Refrigeration at lowest temperatures of the heat cascade are guaranteed by an NH_3 refrigeration cycle (17.3 kg/s of refrigerant is used) operating between (0 °C, 4.3 bar) and (30 °C, 11.7 bar) with a COP of 4.75. The system absorbs 22.7 MW on the evaporator side and releases 20.7 MW heat to 992 kg/s of river water on the condenser side. Water temperature is assumed to change between 23 and 28 °C.

The remaining 304 MW of cold utility is removed from the system at 30 °C with 4278 kg/s of river water.

3. Results

3.1. *Material and energy balance*

In Table 2 the process material balance is displayed. Overall, the process receives 104,167 kg/h of milled corn stover and produces: 7015 kg/h of PA, 567 kg/h of PAc (alongside 85 kg/h of water) which is assumed to be subsequently dehydrated to obtain a full anhydride output stream, 1657 kg/h of MA (98% wt.), 4745 kg/h of FA (90% wt.) and 7794 kg/h of LA (99% wt.). The plant is assumed to operate for 8400 h/y.

Table 2 also displays the monetary flows associated with consumables. The inlet flow of water is the water makeup calculated as a result of the water balance discussed in Section 3.3.

Assumptions on unitary purchase costs and product selling prices are presented in Table A.3.

3.2. *Financial analysis*

From the material and energy balance, a techno-economic analysis of the system was performed. A bottom-up approach

Table 2 – Material balance.

Input	Rate (t/h) or (GJ/h)	Cost (USD/h)
NG (energy basis)	1056.337	6155.44
Feedstock	104.167	5864.30
Water	5.95	1.49
H_2SO_4	4.041	349.19
O_2	0.101	20.91
H_2	0.003	3.34
Cellulase	0.577	1713.81
Isomerase	6.608	2516.87
ACN	0.776	1401.94
MIBK	3.052	9030.70
NH_3	1.078	714.45

Table 3 – Equipment cost.

Item	Reference	Cost (USD)
Pumps	Peters et al. (2004)	1,470,450
Compressors	Peters et al. (2004)	10,951,507
Towers	Peters et al. (2004)	50,978,582
Heat exchangers	Peters et al. (2004)	23,111,168
Evaporators	Peters et al. (2004)	20,147,237
Reactors	Peters et al. (2004)	32,997,821
Filters	Peters et al. (2004)	19,882,913
Power island	IEA-ETSAP (2005)	103,789,114
Total purchased cost		263,328,792
Total installed cost		368,660,309

was used to determine the delivered cost per item of equipment, according to the methodology proposed by Peters et al. (2004). A correction factor was applied to the costs derived from the literature to account for the use of stainless steel material. Installation costs have been estimated as being 40% of the delivered costs. The obtained equipment cost values are reported in Table 3 alongside the corresponding reference.

The cost estimation for the pieces of equipment was developed considering:

- *pumps*: mainly centrifugal pumps were envisaged throughout the process; only the handling of solids and fluids mixture in the pretreatment section included screw feeders;
- *compressors*: 5 compressors are present:
  - two are used for O_2 and H_2 compression and absorb respectively 1.5 and 0.6 MW;
  - one is used for the recovery of MIBK. It absorbs 6 MW and enables the condensation of the solvent gaseous stream at a temperature of 40 °C: the gaseous stream is compressed from 0.013 to 1 atm, thus condensing, and recycled to reactor R6
  - one is used in the MA refining, to compress the overhead vapour from column T10 from the 0.008 to 0.1 atm, before condensing. It absorbs 0.3 MW
  - one is used in the NH_3 refrigeration system and absorbs 5 MW of power
- *columns*: construction details are reported in Table A.2, where the number of stages refers to the theoretical ones in case of trays and to real ones in case of packing. Sieve tray distillation columns have been preferred in presence of streams with tendency to fouling: an overall Murphree efficiency equal to 0.5 was used to calculate the number of real stages from theoretical ones obtained from the simulation. Packing columns have been selected for scrubbers and towers operating under vacuum. In case of high vacuum, Intalox Structured Packing (ISP) has been chosen to reduce the pressure drops;
- *heat exchangers*: the minimum number of heat exchangers was estimated as being 69 and was determined from the number of hot streams, cold streams and utilities placed above and below the pinch as a result of the heat cascade. Then a scaling rule was used to estimate the costs of a set of floating-head heat exchangers, assuming an average exchange area of 40 m^2, as a plausible upper bound on the cost of the heat exchangers;
- *evaporators*: the sets of multiple effects evaporators as described in Sections 2.3–2.4 alongside the one used in the refrigeration cycle, have been modelled in the cost analysis as vertical evaporators;

Table 4 – Total capital investment.

Item	Method (Humbird et al., 2011)	Cost (USD)
ISBL		159,539,678
Warehouse	4% of ISBL	6,381,587
Site development	9% of ISBL	14,358,571
Additional piping	4.5% of ISBL	7,179,286
Total direct cost (TDC)		396,579,753
Prorateable expenses	10% of TDC	39,657,975
Field expenses	10% of TDC	39,657,975
Home office and construction fee	20% of TDC	79,315,951
Project contingency	10% of TDC	39,657,975
Other costs (Start-Up, Permits, etc.)	10% of TDC	39,657,975
Total indirect costs		237,947,852
Fixed capital investment (FCI)		634,527,604
Land	1% of TCI (Peters et al., 2004)	6,729,838
Working capital	5% of FCI	31,726,380
Total capital investment (TCI)		672,983,823

- *reactors*: costs were estimated assigning a residence time for the reaction mix in the reactor. The residence time for the saccharification was assumed 3.5 days (Humbird et al., 2011); the remaining reactions have been assigned a 1 hour residence time, projecting a future increase of efficiencies alongside the scale-up;
- *solid separations*: the solid separators described in Section 2.4 have been modelled in the cost analysis as pressure filters;
- *power island*: the combined-cycle gas turbine system cost was estimated considering an installed capital cost equal to 1100 USD/kWe for 2008 (IEA-ETSAP, 2005). An installation factor equal to 2 was used to calculate the power generation purchased cost.

The index CEPCI (ChemicalEngineering, 2015) was used to update capital cost values with time. Tables 3 and 4 collect respectively the detail of the equipment costs (purchased and installed) and the total capital investment of the process, which turns to be equal to 673 million USD. These preliminary cost estimations are believed to have 30% accuracy.

The breakdown of fixed and variable operating costs is proposed in Table 5. The purification systems for O_2, H_2 and

Table 5 – Total operating costs.

Cost	Method (Humbird et al., 2011)	Value (USD per year)
Utilities		51,705,713
Consumables		132,322,562
Feedstock		49,260,086
Electricity		−82,980,369
Maintenance	3% of ISBL	4,786,190
Insurance	0.7% of FCI	4,441,693
Labour	Scaled with power of 0.2 (Humbird et al., 2011)	5,365,125
Total Product Cost (TPC)		164,901,001

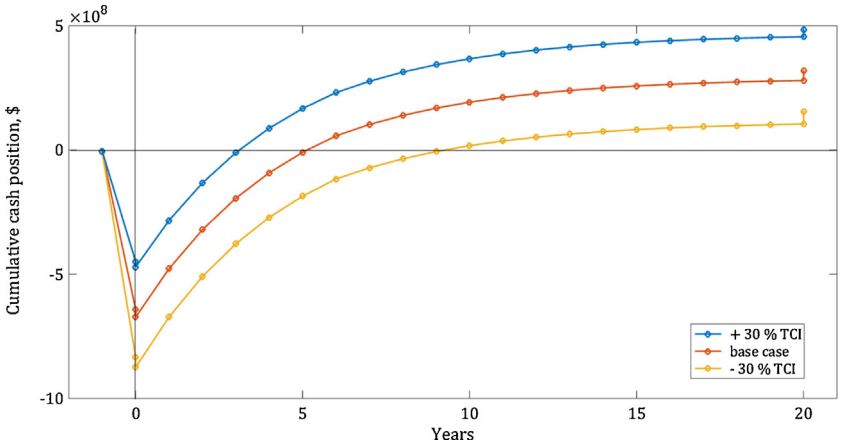

Fig. 4 – PA process: cumulative cash position.

process water were not modelled. In these cases, the material balance was closed assuming:

- 99% recovery for the gaseous streams of reagents was assumed plausible with the exploitation of modern membrane technologies;
- 99% of process water recovery was considered after a waste water treatment composed of anaerobic/aerobic digestion followed by reverse osmosis (Humbird et al., 2011);

The negative cost associated to electricity is due to the net surplus of electricity equal to 152 MW produced in the power island which is assumed to be sold to the grid.

The allocation of the total operating costs over the products rates results in an average production cost of 901.5 USD/t, which is relatively competitive against the current PA market prices.

The financial viability of the process was estimated evaluating the net present value (NPV) of the process, whose cumulative cash position is shown in Fig. 4. Using a minimum acceptable rate of return (MARR) equal to 24% to discount the cash flows, 35% of taxes over profit (Peters et al., 2004) and 6 years for capital depreciation, the NPV was 318 million USD, with 5 years of payback time.

A sensitivity analysis on the capital cost was performed and the effects of capital cost variations were studied. In particular:

- a pessimistic scenario was built up with an increase of capital costs by 30% from the base case and a calculated production cost of 917 USD/t
- an optimistic case was defined with a reduction by 30% of the capital and a production cost of 886 USD/t

Fig. 4 shows the cumulative cash positions for the base case and the scenarios embedding the capital costs variations. Interestingly, the business always shows a positive NPV, equal to 154 and 483 million USD in the pessimistic and optimistic scenario, respectively. Although a shrinkage of profitability occurs in the pessimistic scenario, the internal rate of return (IRR) is still interesting (it reduces from 37% of the base case down to 29%), but the high capital investment could represent a barrier for investors, as the system would be perceived quite riskier having a payback time of 9 years.

3.3. *Environmental considerations: water and CO_2 – eq emissions*

An environmental appraisal has been carried out to estimate the impact on water resources as well as on climate change due to the corn stover-based PA production process simulated in this work. The system boundaries included biomass production and its conversion into products in the plant. Regarding the production of biomass impact factors were calculated assigning the feedstock a residual value. Accordingly, the CO_2 emissions would include the additional portion of fertilisers needed to keep constant crop yields after the residue removal (Giarola et al., 2012). Under these assumptions, water consumption due to biomass growth was neglected, being very small compared to the water used in the process (Bernardi et al., 2013). The effect of logistics was considered outside the scope of the analysis and, thereby, not included.

The water balance in Table 6 shows the relevant share of dilution water, which is especially required for pretreatment, isomerization and saccharification. About 5 t of water are processed per tonne of biomass. About 99.9 % wt. of it is conveyed to the WWT and is mostly recycled.

The water make-up is equal to 5.95 t/h to balance the WWT waste and process vents.

An assessment of the emissions for the production of PA from renewables environment was conducted (Table 7). Emission factors were retrieved from the database Ecoinvent v2.2.

Table 6 – Water balance.

	Rate (t/h)	Share (% wt.)
Input		
biomass	20.83	3.98
H_2SO_4 (93% wt.)	0.28	0.054
Steam	28.98	5.54
Cellulase	0.02	0.004
Dilution	423.82	81.04
Scrubbers	41.81	7.99
Reaction	7.26	1.39
Total	522.99	100.00
Output		
Vent	0.29	0.05
PA	0.09	0.02
FA	0.35	0.07
WWT	522.26	99.86
Total	522.99	100.00

Table 7 – CO_2 emissions.

Input	Emission factor (kg of CO_2 emissions/(t or GJ))	Emissions (kg CO_2 emissions/h)
NG (energy)	1.99 (Frischknecht et al., 2005)	2098.22
Feedstock	53.91 (Giarola et al., 2012)	5615.55
Water	0.675 (Frischknecht et al., 2005)	4.01
H_2SO_4	123.22 (Frischknecht et al., 2005)	497.98
O_2	408.90 (Frischknecht et al., 2005)	41.50
H_2	1661.89 (Frischknecht et al., 2005)	4.49
Cellulase	7000 (Slade et al., 2009)	4039.28
ACN	3042.83 (Frischknecht et al., 2005)	2362.60
MIBK	1761.62 (Frischknecht et al., 2005)	5377.08
NH_3	2096.20 (Frischknecht et al., 2005)	2259.71

They represent emissions from the full product life cycle and refer to the average European market. The total emission allocated to all the products in the portfolio on a mass basis is 1024 kg CO_2/t, which is considerably lower than the conventional process (2534 kg CO_2/t). The impact on global warming due to MIBK was not retrieved from the database and, thus, was estimated using the methylethylketone one.

3.4. *Discussion*

The costs breakdown has shown that the major contributions to the process operating costs are associated to solvents. MIBK and ACN together account for 37% of the total expenses, followed by NG (22%), feedstock (21%), enzymes (15%) and inorganic chemicals (5%) costs.

The large share of operating costs which relates to refining and product purification is due to the solvent rates modelled, replicating the lab scale conditions of the reactions. Consequently, these values must be considered as an upper bound to the separation costs which could be realised with the process scale-up. The same solvents were also characterised by a difficult recovery, challenged by the lower efficiency of extraction compared to other separation systems as well as the tendency of some chemicals involved in the process to form azeotropic mixtures with water (as in the case of ACN).

The relatively high contribution to the total cost of enzymes reflects high uncertainty due to the isomerization contribution. The cost for the glucose isomerase was assumed equal to 1 USD per 100 g of product (fructose) (Ladisch et al., 1977). Due to the lack of more recent data, this value has to be considered an upper bound to current industrial costs. It is worth noting, for example, that cellulase has exhibited a 10-fold cost decrease since the development of the biomass-to-bioethanol process.

In terms of emissions, the key impact comes from the use of solvents (MIBK and ACN account for 35% of the total), by feedstock and cellulase contributions (25 and 18%, respectively), other chemicals (12%) and NG (10%). These results again highlight the need for this process development to increase the concentration of the treated biomass in the pretreatment and, in general, reduce the amount of water handled in the process to improve overall energy efficiency.

4. Concluding remarks

A conceptual design was proposed for the production of phthalic anhydride from milled corn stover. This biorefining system proved to be highly energy intensive due to the low concentration of reactants in the system and the presence of several azeotropes. In order to be economically viable a full portfolio of products was obtained valorising all the carbohydrate fractions (into phthalic anhydride, maleic anhydride, formic acid, levulinic acid) and a pinch analysis was carried out to maximise the energy integration in the system. The lignin is burnt, thus reducing the amount of natural gas fed to the power island. A techno-economic and financial analysis was performed showing that the process would be profitable, although some uncertainty remains in the future market opportunities for formic acid in view of an expansion of biorefining-processes. The life cycle GHG emissions appraisal of the process appears promising compared to the traditional process for the production of PA, although some reliance on fossils would be envisaged, in particular in the combined heat and power section.

Among the major aspects which would require further investigation there would be:

- the cross comparison of alternative separation methods against the extremely energy intensive distillation, particularly when dealing with azeotropic mixtures or unstable species. The case of HMF would be of particular interest: there is only one case of production at industrial scale (AVA, 2015). At the same time, experimental studies show different results regarding performance of the separation process. This would call for additional research to estimate potential product degradation in the proposed flowsheet.
- the evaluation of sensitivity scenarios on solvent consumption reduction, to be stimulated by scaling-up efforts

5. Acknowledgements

The authors would like to thank EPSRC (EP/K014676/1) who funded this work under the Sustainable Chemical Feedstocks programme.

Dr. Francesca Pierobon is kindly thanked for the assistance in the environmental analysis.

Appendix A.

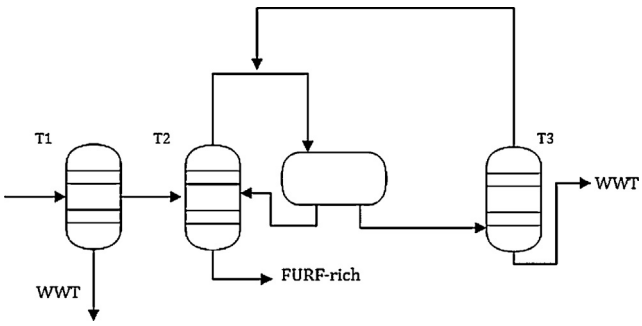

Fig. A.1 – PA process: furfural recovery.

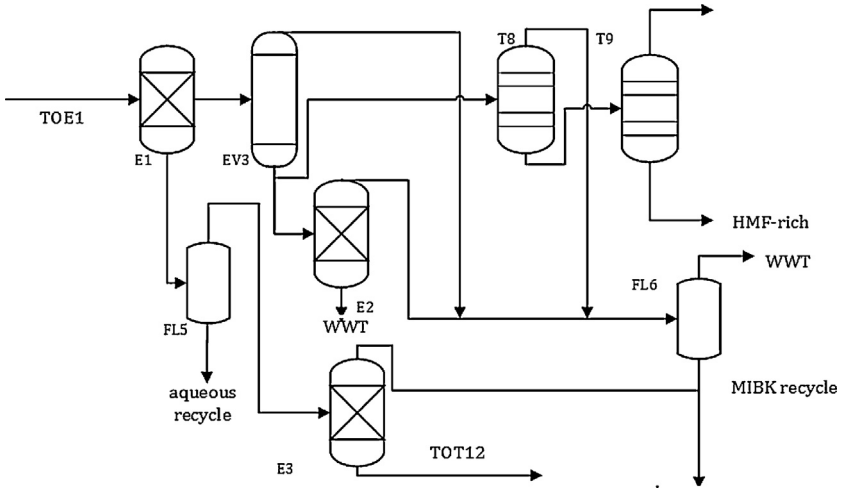

Fig. A.2 – PA process: HMF-MIBK-LA recovery.

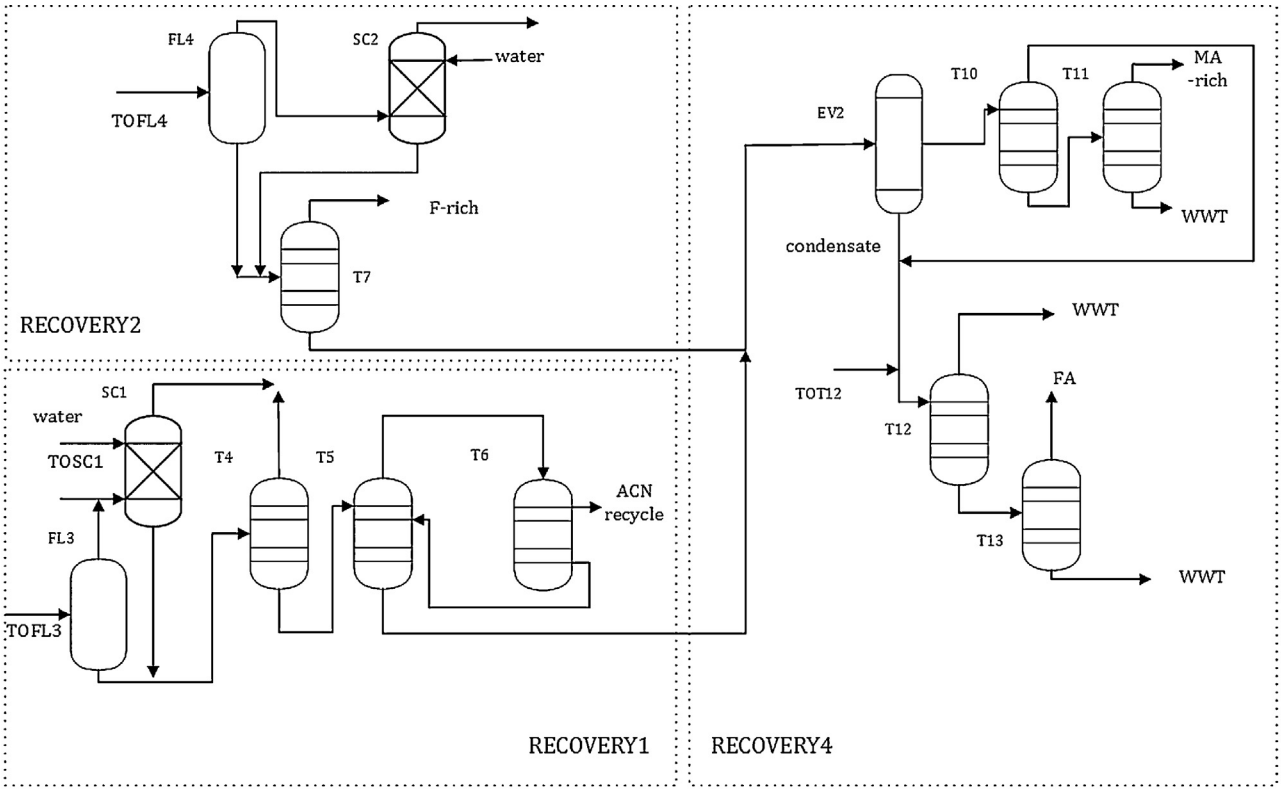

Fig. A.3 – ACN-F-MA-FA recovery.

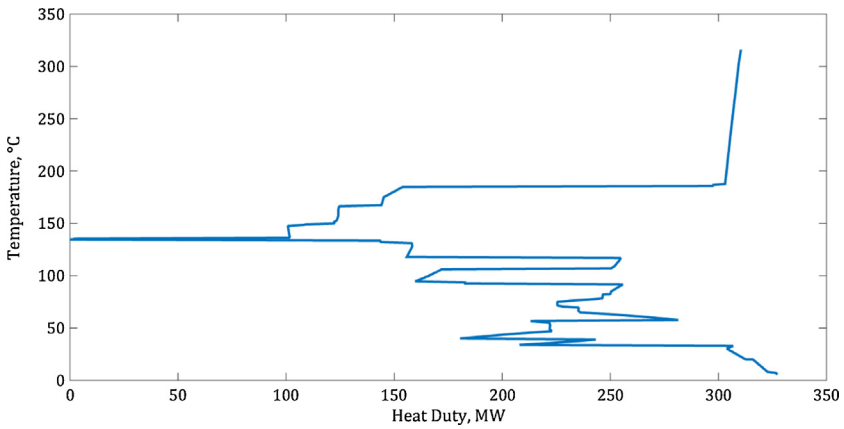

Fig. A.4 – PA process: heat cascade with columns and heat of reactions.

Table. A.1 – Selected reactions.

Reactor tag	Reaction	Temperature (°C)	Pressure (atm)	Reactant	Conversion
M1, M2	(r1)	100, 158	7, 5.7	Cellulose	0.099
M1, M2	(r2)	100, 158	7, 5.7	Cellulose	0.003
M1, M2	(r3)	100, 158	7, 5.7	Xylan	0.9
M1, M2	(r4)	100, 158	7, 5.7	Xylan	0.05
M1, M2	(r5)	100, 158	7, 5.7	Acetate	1
M1, M2	(r6)	100, 158	7, 5.7	HMF	1
M1, M2	(r7)	100, 158	7, 5.7	Furfural	1
M3	(r8)	77.1	5.7	Acetic acid	1
M3	(r9)	77.1	5.7	Sulphuric acid	1
M3	(r10)	77.1	5.7	Xylose	0.01
M4	(r11)	77.4	3.4	Ammonia	1
R1	(r12)	168.5	7.6	Xylose	0.851
R1	(r13)	168.5	7.6	Furfural	0.054
R2	(r14)	319.85	1.1	Furfural	1
R2	(r15)	319.85	1.1	Furan	1
R2	(r16)	319.85	1.1	Furanone	0.84
R3	(r17)	310	1	Furfural	0.909
R3	(r18)	310	1	Furfural	0.032
R3	(r19)	310	1	Furan	0.001
R4	(r20)	48	1	Cellulose	0.9
R5	(r21)	60	1	Glucose	0.589
R6	(r22)	179.85	1	Fructose	0.91
R6	(r23)	179.85	1	HMF	0.4
R7	(r24)	90	1	HMF	0.35
R7	(r25)	90	1	HMF	0.17
R8	(r26)	25	1.5	MA	0.768
R8	(r27)	25	1.5	PA	0.07

Table. A.2 – Columns and extractors specifications.

Tower tag (number)	Overhead, bottom temperature (°C)	Pressure (atm)	Diameter (m)	Stages (ideal)
T1	97.63, 101.40	1	5.4 (SIEVE)	10
T2	99.63, 161.35	1	4.47 (PALL)	10
T3	100.04, 101.03	1.04	1.40 (PALL)	11
SC1	25.14, 31.02	1	1.38 (PALL)	5
T4	96.56, 128.98	2.04	2.65 (PALL)	7
T5(2)	38.94, 51.68	0.23	6.36 (PALL)	7
T6(2)	122.95, 130.31	4.08	5.77 (ISP)	10
SC2	26.77, 44.55	1	1.15 (PALL)	5
T7	75.52, 142.55	3.8	1.71 (SIEVE)	20
E1	24.85, 24.85	1	3.46 (PALL)	5
E2	15, 15	1.3	1.00 (PALL)	5
E3	25, 25	1	2.15 (PALL)	5
T8	76.24, 181.70	0.08	3.07 (PALL)	5
T9(2)	137.10, 143.94	0.013	5.80 (PALL)	60
T10	13.10, 71.10	0.008	4.90 (PALL)	20
T11	76.74, 146.52	0.01	2.55 (PALL)	5
T12(2)	139.52,179.75	6.5	5.74 (SIEVE)	50
T13	41.69, 56.33	0.1	1.90 (PALL)	40

Table. A.3 – Unitary cost.

Item	Source	Unitary cost (USD_{2015}/t) or (USD_{2015}/energy unit)
Biomass	Humbird et al. (2011)	56.30
H_2SO_4	ICIS (2015)	86.40
NH_3	ICIS (2015)	662.75
Enzymes	jbei (2009)	2970
MIBK	ICIS (2015)	2958.60
ACN	ICIS (2015)	1805.59
O_2	chemicool (2015)	206
H_2	chemicool (2015)	1236
Water	Humbird et al. (2011)	0.25
Electricity (kWh)	Humbird et al. (2011)	0.065
NG (GJ)	EIA (2015)	5.83

Item	Source	Selling price (USD_{2015}/t)
FA	Hayes et al. (2008)	121
LA	Hayes et al. (2008)	5850
MA	ICIS (2015)	1805.59
PA	ICIS (2015)	1048.53

References

Alonso-Fagúndez, N., Granados, M.L., Mariscal, R., Ojeda, M., 2012. Selective conversion of furfural to maleic anhydride and furan with vox/al2o3 catalysts. ChemSusChem 5, 1984–1990, http://dx.doi.org/10.1002/cssc.201200167.

Arnold, G., Gross, H., 1964. Furfural solvent separation of aromatics from liquid mixtures. http://www.google.com/patents/US3132093, US Patent 3,132,093.

Arundel, A., Sawaya, D., 2009. The Bioeconomy to 2030, Designing A Policy Agenda.

AVA, 2015. http://www.ava-biochem.com/pages/en/home.php.

Bernardi, A., Giarola, S., Bezzo, F., 2013. Spatially explicit multiobjective optimization for the strategic design of first and second generation biorefineries including carbon and water footprints. Ind. Eng. Chem. Res. 52, 7170–7180, http://dx.doi.org/10.1021/ie302442j.

ChemicalEngineering, 2015. http://www.chemengonline.com/.

Chemicool, 2015. http://www.chemicool.com/elements/hydrogen.html.

Cok, B., Tsiropoulos, I., Roes, A.L., Patel, M.K., 2014. Succinic acid production derived from carbohydrates: an energy and greenhouse gas assessment of a platform chemical toward a bio-based economy. Biofuels Bioprod. Biorefin. 8, 16–29, http://dx.doi.org/10.1002/bbb.1427.

Du, Z., Ma, J., Wang, F., Liu, J., Xu, J., 2011. Oxidation of 5-hydroxymethylfurfural to maleic anhydride with molecular oxygen. Green Chem. 13, 554–557, http://dx.doi.org/10.1039/C0GC00837K.

EC, 2006. The brew project. final report.

EIA, 2015. http://www.eia.gov/naturalgas/.

Frischknecht, R., Jungbluth, N., Althaus, H.-J., Doka, G., Dones, R., Heck, T., Hellweg, S., Hischier, R., Nemecek, T., Rebitzer, G., Spielmann, M., 2005. The ecoinvent database: overview and methodological framework (7 pp.). Int J. Life Cycle Assess. 10, 3–9, http://dx.doi.org/10.1065/lca2004.10.181.1.

Gaily, M.H., Elhassan, B.M., Abasaeed, A.E., Al-shrhan, M., 2010. Isomerization and Kinetics of Glucose into Fructose., pp. 1–6.

Giarola, S., Romain, C., Williams, C.K., Hallett, J.P., Shah, N., 2015. Production of phthalic anhydride from biorenewables: process design. In: Krist, J.K.H., Gernaey, V., Gani, R. (Eds.), 12th International Symposium on Process Systems Engineering and 25th European Symposium on Computer Aided Process Engineering. Elsevier volume 37 of Computer Aided Chemical Engineering, pp. 2561–2566, http://dx.doi.org/10.1016/B978-0-444-63576-1.50121-7 http://www.sciencedirect.com/science/article/pii/B9780444635761501217.

Giarola, S., Shah, N., Bezzo, F., 2012. A comprehensive approach to the design of ethanol supply chains including carbon trading effects. Bioresour. Technol. 107, 175–185, http://dx.doi.org/10.1016/j.biortech.2011.11.090 http://www.sciencedirect.com/science/article/pii/S0960852411017019.

Golden, J., Handfield, R., 2014. Why Biobased? Opportunities in the Emerging Bioeconomy. Technical Report USDA. U.S. Department of Agriculture, Washington, DC.

Haro, P., Ollero, P., Villanueva Perales, A.L., Gómez-Barea, A., 2013. Thermochemical biorefinery based on dimethyl ether as intermediate: technoeconomic assessment. Appl. Energy 102, 950–961, http://dx.doi.org/10.1016/j.apenergy.2012.09.051.

Hayes, D.J., Fitzpatrick, S., Hayes, M.H.B., Ross, J.R.H., 2008. Biorefineries-industrial processes and products. In: The Biofine Process Production of Levulinic Acid, Furfural, and Formic Acid from Lignocellulosic Feedstocks. Wiley-VCH Verlag GmbH, pp. 139–164.

He, J., Zhang, W., 2011. Techno-economic evaluation of thermo-chemical biomass-to-ethanol. Appl. Energy 88, 1224–1232, http://dx.doi.org/10.1016/j.apenergy.2010.10.022.

Humbird, D., Davis, R., Tao, L.C.K., Hsu, A., Aden, D., Schoen, P., Lukas, J., Olthof, B., Worley, M., Sexton, D., Dudgeon, D., 2011. Process Design and Economics for Biochemical Conversion of Lignocellulosic Biomass to Ethanol – Dilute-Acid Pretreatment and Enzymatic Hydrolysis of Corn Stover. http://www.nrel.gov.

ICIS, 2015. http://www.icis.com.

IEA-ETSAP, 2005. http://www.iea-etsap.org/Energy_Technologies/Energy_Supply.asp.

IHS, 2015. https://www.ihs.com.

Ito, T., Yoshida, F., 1963. Vapor–liquid equilibria of water-lower fatty acid systems: Water–formic acid, water acetic acid and water–propionic acid. J. Chem. Eng. Data 8, 315–320, http://dx.doi.org/10.1021/je60018a012.

jbei, 2009. http://econ.jbei.org/index.php/Materials_and_labor.

Kim, S.B., Park, C., Kim, S.W., 2014. Process design and evaluation of production of bioethanol and -lactam antibiotic from lignocellulosic biomass. Bioresour. Technol. 172, 194–200, http://dx.doi.org/10.1016/j.biortech.2014.09.031 http://www.sciencedirect.com/science/article/pii/S0960852414012826.

Ladisch, M.R., Emery, A., Rodwell, V.W., 1977. Economic implications of purfication of glucose isomerase prior to immobilization. Ind. Eng. Chem. Process Design Dev. 16, 309–313, http://dx.doi.org/10.1021/i260063a011.

Lammens, T.M., Gangarapu, S., Franssen, M.C., Scott, E.L., Sanders, J.P., 2012. Techno-economic assessment of the production of bio-based chemicals from glutamic acid. Biofuels Bioprod. Biorefin. 6, 177–187, http://dx.doi.org/10.1002/bbb.349.

Linnhoff, B., Flower, J.R., 1978. Synthesis of heat exchanger networks: I. Systematic generation of energy optimal networks. AIChE J. 24, 633–642, http://dx.doi.org/10.1002/aic.690240411.

Lorz, P., Friedrich, K., Walter, E., Rudolf, J., Naresh, B., Wolfgang, H., 2012. Plastics, General Survey., http://dx.doi.org/10.1002/14356007.a20.

Mahmoud, E., Watson, D.A., Lobo, R.F., 2014. Renewable production of phthalic anhydride from biomass-derived furan and maleic anhydride. Green Chem. 16, 167–175, http://dx.doi.org/10.1039/C3GC41655K.

Mandalika, A., Runge, T., 2012. Enabling integrated biorefineries through high-yield conversion of fractionated pentosans into furfural. Green Chem. 14, 3175–3184, http://dx.doi.org/10.1039/C2GC35759C.

Maslan, F., Stoddard, E., 1956. Acetonitrile + water liquid–vapor equilibrium. J. Phys. Chem. 60, 1146–1147.

mcgroup, 2015. http://mcgroup.co.uk/researches/phthalic-anhydride-pa.

Ozer, R, Vapor phase decarbonylation process. http://www.google.com/patents/US8710251 US Patent 8,710,251.

Peters, M., Timmerhaus, K., West, R., 2004. Plant Design and Economics for Chemical Engineers, 5th ed.

Pick, J., 1972. Phase equilibria in the system tetrahydrofuran (1) -water (2). Collect. Czech. Chem. Commun. 37, 653–2663.

Presson, R., Wu, H., Sockell, E, 1982. Continuous acetonitrile recovery process. http://www.google.com/patents/US4362603 US Patent 4,362,603.

Román-Leshkov, Y., 2014. Phase Modifiers Promote Efficient Production of Hydroxymethylfurfural from Fructose., pp. 1933, http://dx.doi.org/10.1126/science.1126337.

Sikder, J., Roy, M., Dey, P., Pal, P., 2012. Techno-economic analysis of a membrane-integrated bioreactor system for production of lactic acid from sugarcane juice. Biochem. Eng. J. 63, 81–87, http://dx.doi.org/10.1016/j.bej.2011.11.004.

Slade, R., Bauen, A., Shah, N., 2009. The greenhouse gas emissions performance of cellulosic ethanol supply chains in Europe. Biotechnol. Biofuels 2, 15, http://dx.doi.org/10.1186/1754-6834-2-15 http://www.biotechnologyforbiofuels.com/content/2/1/15.

Tang, X., Zeng, X., Li, Z., Hu, L., Sun, Y., Liu, S., Lei, T., Lin, L., 2014. Production of γ-valerolactone from lignocellulosic biomass for sustainable fuels and chemicals supply. Renew. Sustain. Energy Rev. 40, 608–620, http://dx.doi.org/10.1016/j.rser.2014.07.209 http://linkinghub.elsevier.com/retrieve/pii/S1364032114006698.

Trippe, F., Fröhling, M., Schultmann, F., Stahl, R., Henrich, E., 2011. Techno-economic assessment of gasification as a process step within biomass-to-liquid (BtL) fuel and chemicals production. Fuel Process. Technol. 92, 2169–2184, http://dx.doi.org/10.1016/j.fuproc.2011.06.026.

Winkler, M., Romain, C., Meier, M.A.R., Williams, C.K., 2015. Renewable polycarbonates and polyesters from 1,4-cyclohexadiene. Green Chem. 17, 300–306, http://dx.doi.org/10.1039/C4GC01353K.